

# Self- and Mutual Inductance of NbN and Bilayer NbN/Nb Inductors in Planarized Fabrication Process With Nb Ground Planes

Sergey K. Tolpygo, *Senior Member, IEEE*, Evan B. Golden, Terence J. Weir, and Vladimir Bolkhovsky

**Abstract**—We present measurements of self- and mutual inductance of NbN and bilayer NbN/Nb inductors (microstrips, striplines, serpentines, etc.) with Nb ground plane(s) fabricated in an advanced process node developed for superconductor electronics at MIT Lincoln Laboratory. In this process, the signal traces of logic cell inductors are made either of a 200-nm NbN layer with  $T_c \approx 16$  K or of an in-situ deposited NbN/Nb bilayer with 100 /100 nm layer thicknesses, replacing a 200-nm Nb layer M6 in the standard SFQ5ee process with nine superconducting layers on 200-mm wafers. Nb ground planes were preserved to maintain a high level of interlayer shielding and low intralayer mutual coupling. We determined magnetic field penetration depth in the NbN films to be  $\lambda = 491 \pm 5$  nm, corresponding to kinetic inductance of 200-nm films of 1.51 pH/sq. A two-step patterning of the top Nb and the bottom NbN layers of the NbN/Nb bilayer allows to create inductors in a very wide range of linear inductance values, from low values  $\sim 0.4$  pH/ $\mu\text{m}$  typical for Nb geometrical inductors to  $\sim 35$  pH/ $\mu\text{m}$  typical to thin-film kinetic inductors. This is achieved by changing the bilayer linewidth and size of the etched away Nb. Mutual inductance of NbN and Nb inductors, of NbN inductors, and of bilayer inductors is the same as between two Nb inductors with the same geometry and placement between the ground planes, *i.e.*, mutual inductance does not depend on superconducting properties of the signal traces in the studied range of linewidths. Results of the measurements agree with analytical expressions and numerical simulations within a few percent in the studied range of linewidths from 250 nm to 4  $\mu\text{m}$ . Implementation of NbN and NbN/Nb bilayer inductors allows for a significant increase in the circuit density and integration scale of superconductor digital electronics.

**Index Terms**—Please choose four to five keywords or phrases in alphabetical order, separated by commas. A hierarchical list of terms is given in the IEEE Taxonomy located online at [https://www.ieee.org/documents/taxonomy\\_v101.pdf](https://www.ieee.org/documents/taxonomy_v101.pdf)

## I. INTRODUCTION

**A**DVANTAGES superconductor digital electronics over semiconductor electronics in clock frequency and energy efficiency are well known. However, a three to four orders of magnitude lower scale of integration of superconductor electronics (SCE) compared to CMOS impedes SCE applications. The main limiting factor to the integration scale is the size of

Josephson junctions (JJs) and inductors in logic and memory cells [1].

The current trend of SCE development is towards lowering energy dissipation, which is achieved by decreasing the typical critical current  $I_c$  of JJs and hence of their area. This in turn increases inductance values, and area, of all inductors in the cells because their typical inductance  $L$  relates to  $I_c$  through the cell design parameter  $\beta_L = 2\pi LI_c / \Phi_0$  determined in the cell simulation and optimization [2]. Another trend of the last decade is proliferation of multiphase ac clocked logics utilizing either bipolar switching of JJs as in RQL logic [3] or quasi-adiabatic changes in the flux state of logic cells as in AQFP [4], [5]. In addition to regular cell inductors, ac-clocked circuits require efficient cell transformers (mutual) inductors to couple the ac excitation. These transformers are poorly scalable as explained in [6], [7].

It is also well known [1] that area occupied by cell inductors can be substantially decreased if Nb inductors in integrated circuits, which are mainly magnetic (geometrical) inductors, could be replaced by kinetic inductors – thin films of materials with large magnetic field penetration depth  $\lambda \gg t$  giving rise to kinetic inductance  $L_{Ksq} = \mu_0 \lambda^2 / t \approx 1.257 \lambda^2 / t$  (in pH per square for  $\lambda, t$  in  $\mu\text{m}$ ) that is much larger than magnetic inductance  $L_m$ , where  $t$  is the film thickness. Such materials are also well known, e.g., thin films of NbN, NbTiN, Mo<sub>2</sub>N [2], and can theoretically replace Nb layers in a multi-layer stack of the existing fabrication processes [8]–[10].

However, implementing kinetic inductors would significantly decrease mutual inductance in transformers because reducing length of inductors would also decrease their mutual running length. So, superconductor logics and memories utilizing ac excitation may not necessarily benefit from implementation of kinetic inductors.

It is also clear that all Nb layers in the process stack cannot be replaced by superconducting materials having much larger penetration depth than  $\lambda_{\text{Nb}} = 90$  nm because this would dramatically compromise screening properties of the ground planes, increase parasitic coupling between inductors, increase

Manuscript receipt and acceptance dates will be inserted here. This material is based upon work supported by the Under Secretary of Defense for Research and Engineering under Air Force Contract No. FA8702-15-D-0001. Distribution statement A. Approved for public release. Distribution is unlimited. (*Corresponding author: Sergey K. Tolpygo.*)

All authors are with Lincoln Laboratory, Massachusetts Institute of Technology, Lexington, MA 02421, USA (e-mails: [sergey.tolpygo@ll.mit.edu](mailto:sergey.tolpygo@ll.mit.edu), [evan.golden@ll.mit.edu](mailto:evan.golden@ll.mit.edu), [weir@ll.mit.edu](mailto:weir@ll.mit.edu), [blokv@ll.mit.edu](mailto:blokv@ll.mit.edu)).

Color versions of one or more of the figures in this paper are available online at <http://ieeexplore.ieee.org>.

Digital Object Identifier will be inserted here upon acceptance.

impedance of and delay in passive transmission lines (PTLs), etc. Therefore, materials with high kinetic inductance can replace Nb only on some dedicated inductor layers while Nb must be preserved on all layers used for ground planes and PTLs.

Despite a clear need for kinetic inductors for increasing integration scale, we are not aware of their implementations in logic cells of superconductor integrated circuits. In the SFQ5ee process at MIT LL, 40-nm-thick films of Mo<sub>2</sub>N with inductance of 8 pH/sq [11] are only used as rf choke inductors in a voltage biasing scheme of ERSFQ circuits [12], [13].

In this work we describe properties of inductors made of 200-nm-thick NbN films and bilayers NbN/Nb incorporated as the inductor layer in the process stack of the SFQ5ee process [9], [10] with 8 planarized niobium layers, replacing Nb layer M6.

The use of NbN/Nb bilayers allows us to combine kinetic inductors and magnetic (geometrical) inductors on the same circuit level and thereby preserve the required mutual inductance in transformers and provide compact kinetic inductors in logic cells.

## II. FABRICATION PROCESS AND MEASUREMENTS

### A. The SFQ5ee Process with NbN Layer M6

Process flow of the standard SFQ5ee process with 8 niobium planarized layers on 200-mm wafers, described in [9], [10], was used up to the metal layer M6, the layer interconnecting Josephson junctions and shunt resistors; see [14, Fig. 1], [9, Fig. 1], [10, Fig. 1]. At this step, a 200-nm-thick NbN layer was deposited (instead of Nb) using reactive sputtering of Nb in Ar/N<sub>2</sub> flow, in one of the deposition chambers of an Endura PVD cluster tool. After the standard 248-nm photolithography, NbN layer M6 was patterned using high-density plasma etching in Cl<sub>2</sub>-based chemistry. The patterned layer was planarized using SiO<sub>2</sub> deposition and chemical mechanical polishing, forming interlayer dielectric, I6. Two dielectric thicknesses were used: 200 nm on wafer #9 (w9), as in the standard process; and 100 nm on wafer #10 (w10). The latter was done to increase mutual coupling between inductors on the layers M6 and M7. Then, Nb layer M7 was deposited and patterned as in the standard SFQ5ee process, followed by the wafer surface passivation and contact pad metallization steps completing the process flow. This process modification does not require any additional photomasks or processing steps in comparison to the SFQ5ee process.

### B. The SFQ5ee Process with NbN/Nb Bilayer as Layer M6

Similar to II.A, after reaching deposition step of the layer M6, it was deposited in-situ as NbN/Nb bilayer with total thickness of 200 nm. Thicknesses of the individual layers  $t_{NbN}$  and  $t_{Nb}$  were varied to investigate various combinations, although the main interest present equal thicknesses  $t_{NbN} = t_{Nb} = 100$  nm.

Patterning of the bilayer is shown in Fig. 1 and done in two photolithography and etching steps to pattern individually the top Nb and the bottom NbN layers of the bilayer. The first photolithography step uses a dark field mask M6a and positive

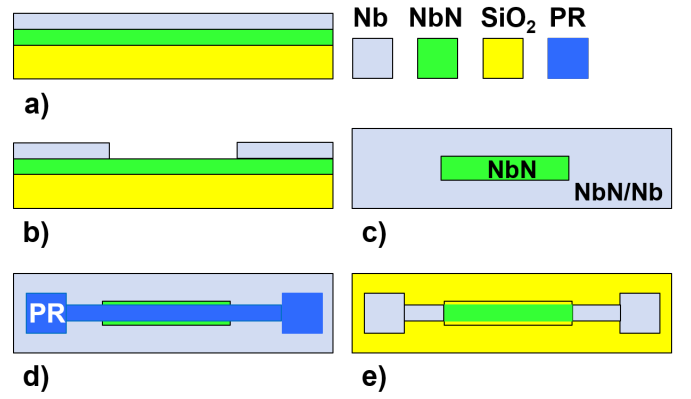


Fig. 1. Processing of the NbN/Nb bilayer: a) cross section of a bilayer deposited on a planarized layer of SiO<sub>2</sub> interlayer dielectric, I5 (between layers M5 and M6); b) patterning of the top Nb layer, using a dark field mask M6a and selective etching of Nb over NbN; c) top view of the etched structure; d) second photolithography step uses a clear field mask M6 to define the inductor shape; e) top view after etching NbN/Nb bilayer (not protected by the photoresist mask) down to the SiO<sub>2</sub> dielectric. These steps produce a composite inductor consisting of NbN central part (green), aligned in the window etched in Nb in the step c), and the NbN/Nb bilayer parts (grey) providing low inductance connections to the high kinetic inductance NbN.

photoresists (PR). This step does not exist in the standard SFQ5ee process, and creates unmasked etch windows for etching the top Nb of the bilayer in the regions where NbN inductors are going to be placed. After selectively etching the top Nb in the unmasked areas, the second photolithography is done using a clear field M6 and positive PR; Fig.1d. Then, the bilayer is etched off from all unmasked area in one etching step, stopping on the underlying SiO<sub>2</sub>; see Fig. 1e. As a result of this two-step patterning, we formed variable thickness inductors consisting of a thin NbN part or several parts and thick parts consisting of the full bilayer. After that, the process layer stack is completed as II.A by Nb layer M7.

### C. Inductance and Mutual Inductance Measurements

Inductance and mutual measurements were done using a SQUID-based method [15] and integrated circuit developed in [16, Fig. 4], and discussed in detail in [17]. Extensive data on Nb microstrip and stripline inductors as well as analytical expressions were given in [18]. In all cases, we measured the differential inductance of two arms of the SQUID, differing only

TABLE I  
PARAMETERS OF LAYERS IN MEASURED INDUCTORS

Parameter	w9 (nm)	w10 (nm)
Nb ground plane layer M4 thickness (nm)	200	200
Nb layer M5 thickness	135	135
Dielectric thickness between layers M4 and M5	200	200
Dielectric thickness between layers M4 and M6	615	615
NbN layer M6 thickness	200	200
Dielectric thickness between layers M6 and M7	200	100
Dielectric thickness between layers M4 and M7	1015	915
Nb layer M7 thickness	200	200
Magnetic field penetration depth in Nb films	90	90

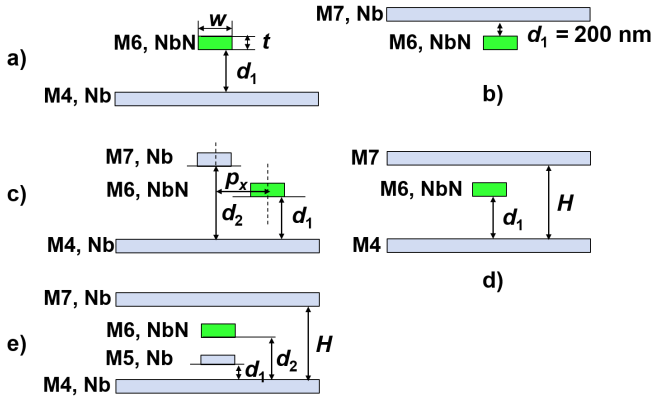


Fig. 2. Cross sections of the inductors studied: a) microstrips M6aM4 (standing for a microstrip with signal trace on the layer M6 above the M4 ground plane); b) inverted microstrip M6bM7 (“bM7” stands for below the M7 ground plane); c) mutual coupling of microstrip inductors M6aM4 and M7aM4,  $p_x$  is the distance between geometrical centers of the signal traces in the horizontal, x-direction; d) stripline inductor M6aM4bM7; e) mutual coupling of striplines M5aM4bM7 and M6aM4bM7; distance between their geometrical center was varied. Dielectric thicknesses entering analytical expressions in the text are also indicated.

by the length of inductors, in order to remove all parasitic contributions. The measured values were normalized to the length difference, 45  $\mu\text{m}$ , giving self-inductance,  $L_l$  or mutual inductance,  $M_l$  per unit length. Nominal thicknesses of dielectric and superconducting layers involved in the studied inductors are given in Table I. Cross sections of the typical inductors and mutual inductors studied are sketched in Fig. 2.

### III. RESULTS

#### A. Inductance of NbN Microstrips with Nb Ground Planes

Inductance of NbN microstrips M6aM4, Fig. 2a, and M6bM7, Fig. 2b, per unit length is shown in Fig. 3 for microstrips of various widths,  $w$ . For a comparison, we give data for Nb microstrips of the same types, fabricated on a different wafer in the same process run. Obviously, inductance of the microstrips with NbN signal traces is much larger than of microstrips with the same geometry but with Nb traces.

According to [18], inductance of superconducting microstrips per unit lengths is given by

$$L_l = \frac{\mu\mu_0}{4\pi} \ln \left[ 1 + \frac{4(d_1 + \frac{t_1}{2} + \lambda)^2}{0.2235^2(w + t_1)^2} \right] + \frac{\mu_0\lambda_1^2}{t_1w}, \quad (1)$$

where  $\lambda$  and  $\lambda_1$  are magnetic field penetration depths in, respectively, the ground plane(s) and the signal trace materials;  $\mu_0 = 4\pi \times 10^{-7} \text{ H}\cdot\text{m}^{-1}$  and  $\mu$  are, respectively, the vacuum and relative magnetic permeability; the latter is assumed equal unity in all the calculations hereafter. The first term in (1) is magnetic part of the inductance, which depends on the penetration depth in the ground plane. The second term is kinetic inductance, assuming a uniform current distribution in the signal trace. source file should contain all figures and tables at the submission Fitting to (1) of the experimental data on the microstrips with three different values of  $d_1 = 615 \text{ nm}$ ,  $200 \text{ nm}$ , and  $100 \text{ nm}$  is shown

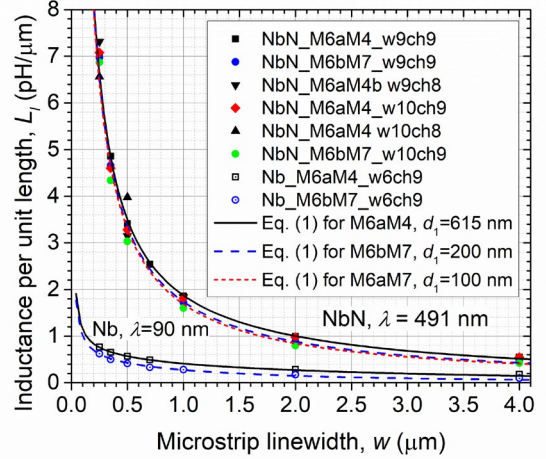


Fig. 3. Inductance per unit length of microstrips M6aM4 and inverted microstrips M6bM7 using 200-nm NbN layer M6 and Nb ground planes M4 or M7 as a function of linewidth of the NbN signal traces,  $w$ . Data for two wafers, w9 and w10, and two 5 mm  $\times$  5 mm chips, ch8 and ch9, at two locations on 200-nm wafers are given. For a comparison, the data are also given for fully Nb microstrips co-fabricated in the same process run on wafer #6 (w6) on the same chips and locations on the wafer. Solid and dash curves are fits to (1), giving magnetic field penetration depth in NbN  $\lambda_1 = 491 \pm 5 \text{ nm}$  at magnetic field penetration depth in Nb ground planes of  $\lambda = 90 \text{ nm}$ ; see the two bottom curves for Nb. Short dash magenta curve is also a fit to (1) but at a different dielectric thickness  $d_1 = 100 \text{ nm}$  between the layers M6 and M7 on w10.

in Fig. 3, and given a mean value of magnetic field penetration depth in NbN films  $\lambda_1 = 491 \pm 5 \text{ nm}$ . This translates into a sheet inductance of 200-nm NbN films of 1.51 pH/sq. Consequently, 100-nm-thick NbN films should have  $2\times$  higher sheet inductance, about 3.0 pH/sq.

#### B. Inductance of NbN Striplines M6aM4bM7 with Nb Ground Planes

Inductance per unit length of NbN striplines M6aM4bM7 with Nb ground planes M4 and M7 is shown in Fig. 4, along with fully Nb striplines for a comparison. Similar to the microstrips in Fig. 3, inductance of NbN striplines is many times larger than of the Nb striplines with the same dimensions.

Superconducting stripline inductance is given in [18] by

$$L_l = \frac{\mu\mu_0}{4\pi} \ln \left( 1 + \frac{\sin^2 \pi \left( d_1 + \frac{t_1}{2} + \lambda \right)}{\frac{H+2\lambda}{\pi r_{eq}}} \right) + \frac{\mu_0}{8\pi} + \frac{\mu_0\lambda_1^2}{t_1w}, \quad (2)$$

where  $r_{eq}$  is the equivalent radius of the rectangular cross section given in [18, (23a)] and [8, (23b)], and  $H$  is the dielectric thickness between the ground planes; see Fig. 2d. The sum of the first two terms in (2) is magnetic inductance of the stripline, and the third term is kinetic inductance of the signal strip. This expression with the penetration depths determined from the fits in Fig. 3, is plotted in Fig. 4 for NbN striplines (solid black curve) and Nb striplines (dash black curve), and gives an excellent description of the data.

Instead of the equivalent radius approximation (2), magnetic component of the stripline inductance can be also expressed using Maxwell’s geometric mean distance method [19]–[21], calculating self-inductance as mutual inductance of the rectangular

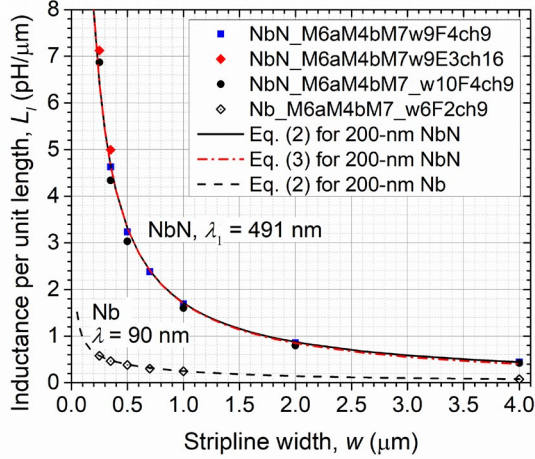


Fig. 4. Inductance per unit length of striplines M6aM4bM7 (Fig. 2d) using 200-nm NbN layer M6 and Nb ground planes M4 and M7 as a function of linewidth of the NbN signal traces,  $w$ . Data on two wafers, w9 and w10, and two 5 mm  $\times$  5 mm chips, ch9 and ch16, at two locations, F4 and E3, on 200-mm wafers are given. For a comparison, the data are also given for Nb striplines fabricated in the same process run on wafer #6 (w6). Solid black curve is (2) at magnetic field penetration depth in NbN  $\lambda_1 = 491$  nm and  $\lambda = 90$  nm in all the Nb layers;  $H = 1015$  nm,  $d_1 = 615$  nm; see Table I. Red dash-dot curve is (3) at the same parameters. Dash curve is (2) for Nb striplines at  $\lambda_1 = \lambda = 90$  nm.

cross section with itself placed at the geometrical mean distance, giving,

$$L_l = \frac{\mu\mu_0}{4\pi} \ln \left( 1 + \frac{\sin^2 \pi \left( d_1 + \frac{t_1}{2} + \lambda \right)}{\sinh^2 \frac{0.2235\pi(w+t)}{2(H+2\lambda)}} \right) + \frac{\mu_0 \lambda_1^2}{t_1 w}, \quad (3)$$

where  $0.2235(w+t_1)$  is Maxwell's geometrical mean distance for a rectangle; see [20, (124)]. Expression (3) is also plotted in Fig. 4 by the dash-dot red curve. It gives nearly identical values to (2) up to  $w = 1$   $\mu\text{m}$  and somewhat lower inductance at larger linewidth; the difference is  $-3\%$  at  $w = 2$   $\mu\text{m}$ , gradually increasing to  $-9\%$  at  $w = 4$   $\mu\text{m}$ . It is clear that both (2) and (3) can be used to calculate inductance of NbN striplines in the ranges of linewidths important for inductors in superconductor integrated circuits,  $w \leq 2$   $\mu\text{m}$ , within the accuracy of the experimental data and parameters spread across 200-mm wafers.

### C. Mutual Inductance of NbN and Nb Microstrips

Mutual inductance between Nb microstrip M7aM4 and NbN microstrip M6aM4 is shown in Fig. 5 as a function of horizontal distance between the geometrical centers of the microstrips' cross sections,  $p_x$ ; see Fig. 2c. The linewidths of both microstrips are equal and  $w_1 = w_2 = 250$  nm. For a comparison, also shown is mutual inductance for all-Nb microstrips of the same width (open dots) fabricated on the wafer #6. Within error of the measurements and wafer-to-wafer variation, there is no difference between the mutual inductance of the NbN–Nb pair and Nb–Nb pair of the microstrips. The measurements confirm that the mutual inductance matrix is symmetrical in all the cases described hereafter.

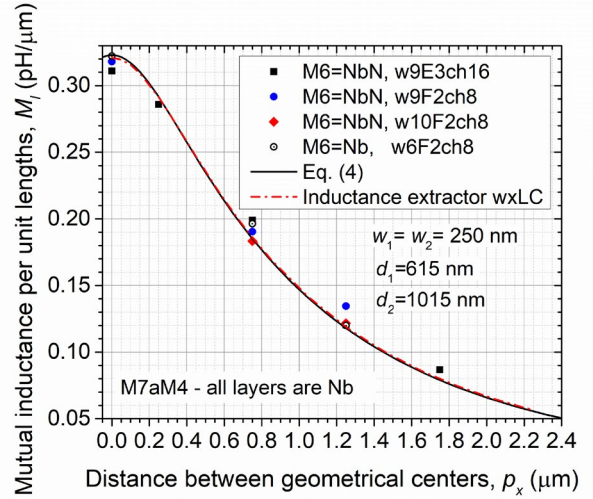


Fig. 5. Mutual inductance per unit length of Nb microstrips M7aM4 and NbN microstrips M6aM4 with equal width  $w = 250$  nm as a function of horizontal spacing between the geometrical centers of microstrip cross sections,  $p_x$ ; see Fig. 2c. For a comparison, the data are also given for all-Nb microstrips fabricated in the same process run on wafer #6 (w6). Solid black curve is (4) at magnetic field penetration depth in the Nb ground plane  $\lambda = 90$  nm and  $d_1 = 615$  nm, and  $d_2 = 1015$  nm; see Table I. Red dash-dot curve shows numerical simulation done using inductance extractor wxLC [22] at the same parameters.

Mutual inductance of two superconducting microstrips with thicknesses  $t_1$  and  $t_2$ , dielectric thicknesses  $d_1$  and  $d_2$ , and linewidths  $w_1, w_2 \lesssim |d_2 - d_1|$  is given in [18] by

$$M_l = \frac{\mu\mu_0}{4\pi} \ln \left[ 1 + \frac{4(d_1 + \lambda + \frac{t_1}{2})(d_2 + \lambda + \frac{t_2}{2})}{p_x^2 + (d_2 - d_1 + \frac{t_2 - t_1}{2})^2} \right]. \quad (4)$$

It is plotted in Fig. 5 by the solid black curve and describes the experimental data very well. For a comparison, we also show by the dash-dot red curve the results of mutual inductance extraction using wxLC software for a transmission line approximation developed by M. Khapaev [22]. At small linewidths, (25) is virtually indistinguishable from the numerical results. We note that  $M_l$  decays slowly with increasing the distance between the microstrips, only as a second power of the distance. This gives rise to a large parasitic mutual coupling of inductors in dense circuits.

### D. Mutual Inductance of NbN and Nb Striplines

Mutual inductance of NbN striplines M6aM4bM7 and Nb striplines M5aM4bM, see Fig. 2c, of equal width  $w_1 = w_2 = 250$  nm is shown in Fig. 6. The measurements confirm that the mutual inductance matrix is symmetrical. Note that mutual inductance of the striplines is much smaller than mutual inductance of microstrips in Fig. 5 and is more difficult to measure as a result.

Mutual inductance of superconducting striplines is given in [18] by

$$M_l = \frac{\mu\mu_0}{4\pi} \ln \frac{\cosh \frac{\pi p_x}{H+2\lambda} \cos \frac{\pi(d_1+d_2+t_1+t_2+2\lambda)}{H+2\lambda}}{\cosh \frac{\pi p_x}{H+2\lambda} \cos \frac{\pi(d_2-d_1+t_2-t_1)}{H+2\lambda}}. \quad (5)$$

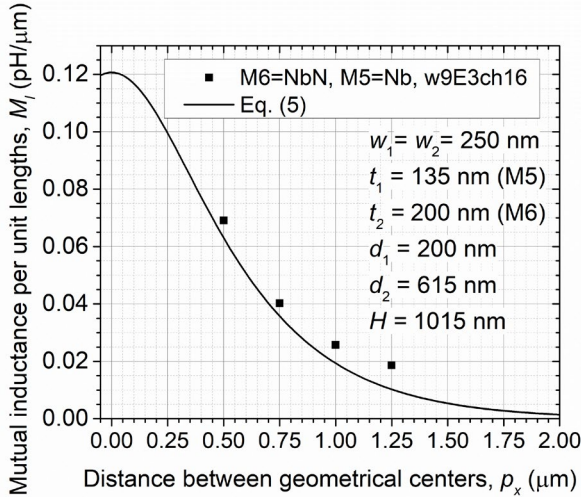


Fig. 6. Mutual inductance per unit length of Nb stripline M5aM4bM7 and NbN stripline M6aM4bM7 with equal width  $w = 250$  nm as a function of horizontal spacing between the geometrical centers of their cross sections,  $p_x$ ; see Fig. 2e. Solid black curve is (5) at magnetic field penetration depth in the Nb ground plane  $\lambda = 90$  nm and  $d_1 = 200$  nm,  $d_2 = 615$  nm, and  $H = 1015$  nm; see Table I.

It is plotted in Fig. 6 for the parameters of the striplines used and provides a reasonable description of the experimental data. We believe that progressively increasing difference between the experiment and (5) with increasing  $p_x$  is likely a result of experimental difficulties with measuring small mutual inductances. This requires applying large modulation currents through the primary inductor M5 forming a transformer with a large NbN inductor M6 in the SQUID arm.

#### E. Self- and Mutual Inductance of NbN/Nb Bilayers

Inductance of NbN and Nb layers of the bilayer are given by (1) or (2) with appropriate thicknesses. For instance, for the bilayer M6 (biM6) with  $t_{NbN} = t_{Nb} = 100$  nm,  $d_1 = 615$  nm and 715 nm for NbN and Nb layers, respectively. Since  $\lambda_1 \gg \lambda$ , inductance of NbN layer is much larger than of Nb layer. Hence, inductance of the parallel combination of these layers in the bilayer is approximately equal to the inductance of the top Nb layer. Mutual inductance between microstrips or striplines in the bilayer or between the bilayer and Nb, or between inductors in the bottom NbN layer and other inductors can be calculated using (4) and (5) or more general expressions in [18], or simulated using inductance extractors wxLC or InductEx [23]. Some results of these simulations are given in [24], and results of the measurements will be given elsewhere.

#### IV. DISCUSSION OF THE RESULTS

The main goals of this work were to show that kinetic inductors can be implemented in a multilayered fabrication process and used as cell inductors in digital mixed signal integrated circuits. Our measurements give necessary data for circuit design.

Very thin NbN films have been widely used for single layer photon counters – superconducting nanowire single photon detectors (SNSPDs) [25]–[28] and microwave kinetic inductance

detectors (MKIDs); see [29] and references therein. Penetration depth in thick NbN films deposited using reactive sputtering [30] at 280 °C was measured, e.g., in [31] and found to be 370 nm from the microwave measurements. The large difference with the penetration depth measured on our NbN films can be ascribed to the large difference in the deposition temperature and resistivity of the films.

Other convenient material for incorporation in our process and integration with Nb/Al-AIO<sub>x</sub>/Nb junctions could be NbTiN films [32]–[35], which have a smaller penetration depth than NbN, in the range from 230 nm to 360 nm, depending on the deposition conditions [33], [35].

#### V. CONCLUSION

We presented inductance and mutual inductance data for NbN microstrips and striplines with  $T_c \approx 16$  K incorporated in a fully planarized multilayered fabrication process with Nb ground planes and Nb/Al-AIO<sub>x</sub>/Nb Josephson junctions, an advanced node of the standard SFQ5ee process. We also presented a different node of this process, which uses NbN/Nb bilayers to form compact inductors in logic cells of digital and mixed signal integrated circuits. Presented data should be sufficient for circuit design in these advanced nodes of superconductor electronics processes at MIT LL.

One the main beneficiaries of kinetic inductors will be energy-efficient integrated circuits using Josephson junction with low critical currents, below about 50  $\mu\text{A}$ , which require large inductance values of their cell inductors. For instance, superconductor neuromorphic circuits have recently become a subject of hot interest; see a review [36] and references therein. Many types of neuromorphic circuits process information in a stochastic manner and are much less sensitive to bit error rates than digital circuits; see e.g., [37]–[39]. Hence, critical currents of JJs in them, and energy dissipation, can be substantially lowered with respect to the typical critical currents used in digital circuits,  $I_c \sim 100$   $\mu\text{A}$ , down to 10–20  $\mu\text{A}$ , and inductances proportionally increased using the approach described above.

Full implementation of NbN/Nb bilayer inductors should provide for a 10x increase in the inductor number density and hence significantly increase integration scale of superconductor electronics.

#### ACKNOWLEDGMENT

We are grateful to Vasili Semenov for numerous discussions of bilayer inductors and neuromorphic circuits, and to Ravi Rastogi for his help in wafer processing. S.K. Tolpygo would like to thank Mikhail M. Khapaev for the access to inductance extraction software wxLC, and to Coenrad J. Fourie for the access to and help with InductEx. We would like to thank Leonard Johnson and Mark Gouker their interest in this work.

This research was based upon work supported by the Under Secretary of Defense for Research and Engineering via Air Force Contract No. FA8702-15-D-0001. Any opinions, findings, conclusions or recommendations expressed in this material are those of the authors and do not necessarily reflect the

views of the Under Secretary of Defense for Research and Engineering and should not be interpreted as necessarily representing the official policies or endorsements, either expressed or implied, of the U.S. Government. Delivered to the U.S. Government with Unlimited Rights, as defined in DFARS Part 252.227-7013 or 7014 (Feb 2014). Notwithstanding any copyright notice, U.S. Government rights in this work are defined by DFARS 252.227-7013 or DFARS 252.227-7014 as detailed above. Use of this work other than as specifically authorized by the U.S. Government may violate any copyrights that exist in this work. The U.S. Government is authorized to reproduce and distribute reprints for Governmental purposes notwithstanding any copyright annotation thereon.

## REFERENCES

- [1] S.K. Tolpygo, "Superconductor electronics: scalability and energy efficiency issues," *Low Temp. Phys. / Fizika Nizkikh Temperatur*, vol. 42, no. 5, pp. 463-485, May 2012.
- [2] K.K. Likharev and V.K. Semenov, "RSFQ logic/memory family: a new Josephson-junction technology for sub-terahertz-clock-frequency digital systems," *IEEE Trans. Appl. Supercond.*, vol. 1, no. 1, pp. 3-28, Mar. 1991
- [3] Q.P. Herr, A.Y. Herr, O.T. Oberg, and A.G. Ioannidis, "Ultra-low-power superconducting logic," *J. Appl. Phys.*, vol. 109, 2011, Art. no. 103903.
- [4] Y. Harada, H. Nakane, N. Miyamoto *et al.*, "Basic operation of quantum flux parametron," *IEEE Trans. Magn.*, vol. MAG-23, no. 5, pp. 3801-3807, Sep. 1987.
- [5] N. Takeuchi, D. Ozawa, Y. Tamanashi, and N. Yoshikawa, "An adiabatic quantum flux parametron as an ultra-low-power logic device," *Supercond. Sci. Technol.*, vol. 26, no. 3, Mar. 2013, Art. no. 035010.
- [6] S. K. Tolpygo, E. B. Golden, T. J. Weir and V. Bolkhovskiy, "Mutual and self-inductance in planarized multilayered superconductor integrated circuits: Microstrips, striplines, bends, meanders, ground plane perforations," *IEEE Trans. Appl. Supercond.*, vol. 32, no. 5, pp. 1-31, Aug. 2022, Art. no. 1400331, doi: 10.1109/TASC.2022.3162758.
- [7] S.K. Tolpygo, "Scalability of superconductor electronics: limitations imposed by ac clock and flux bias transformers," *arXiv preprint arXiv: 2210.02632*; submitted to *IEEE Trans. Appl. Supercond.*
- [8] S. Nagasawa, K. Hinode, T. Satoh *et al.*, "Nb 9-layer fabrication process for superconducting large-scale SFQ circuits and its process evaluation," *IEICE Trans. Electron.*, vol. E97-C, No. 3, pp. 132-140, Mar. 2014.
- [9] S. K. Tolpygo *et al.*, "Advanced fabrication processes for superconducting very large-scale integrated circuits," *IEEE Trans. Appl. Supercond.*, vol. 26, no. 3, pp. 1-10, Apr. 2016, Art. no. 1100110, doi: 10.1109/TASC.2016.2519388.
- [10] S.K. Tolpygo *et al.*, "Fabrication processes for superconductor electronics: Current status and new developments," *IEEE Trans. Appl. Supercond.*, vol. 29, no. 5, pp. 1-13, Aug. 2019, Art. no. 1102513, doi: 10.1109/TASC.2019.2904919.
- [11] S. K. Tolpygo *et al.*, "Superconductor electronics fabrication process with MoN<sub>x</sub> kinetic inductors and self-shunted Josephson junctions," *IEEE Trans. Appl. Supercond.*, vol. 28, no. 4, pp. 1-12, June 2018, Art. no. 1100212, doi: 10.1109/TASC.2018.2809442.
- [12] D. E. Kirichenko, S. Sarwana and A. F. Kirichenko, "Zero static power dissipation biasing of RSFQ circuits," *IEEE Trans. Appl. Supercond.*, vol. 21, no. 3, pp. 776-779, June 2011, doi: 10.1109/TASC.2010.2098432
- [13] M. E. Çelik *et al.*, "25-GHz Operation of ERSFQ time-to-digital converter," *IEEE Trans. Appl. Supercond.*, vol. 31, no. 5, pp. 1-5, Aug. 2021, Art. no. 1301805, doi: 10.1109/TASC.2021.3065282.
- [14] S. K. Tolpygo, V. Bolkhovskiy, T. J. Weir, L. M. Johnson, M. A. Gouker and W. D. Oliver, "Fabrication process and properties of fully-planarized deep-submicron Nb/Al-AIO<sub>x</sub>/Nb Josephson junctions for VLSI circuits," *IEEE Trans. Appl. Supercond.*, vol. 25, no. 3, pp. 1-12, June 2015, Art. no. 1101312, doi: 10.1109/TASC.2014.2374836.
- [15] W.H. Henkels, "Accurate measurement of small inductances or penetration depths in superconductors," *Appl. Phys. Lett.*, vol. 32, pp. 829-831, 1978.
- [16] S. K. Tolpygo *et al.*, "Inductance of circuit structures for MIT LL superconductor electronics fabrication process with 8 niobium layers," *IEEE Trans. Appl. Supercond.*, vol. 25, no. 3, pp. 1-5, June 2015, Art. no. 1100905, doi: 10.1109/TASC.2014.2369213.
- [17] S.K. Tolpygo, E.B. Golden, T.J. Weir, and V. Bolkhovskiy, "Inductance of superconductor integrated circuit features with sizes down to 120 nm," *Supercond. Sci. Technol.*, vol. 34, no. 8, June 2021, Art. no. 085005, doi: 10.1088/1361-6668/ac04b9
- [18] S. K. Tolpygo, E. B. Golden, T. J. Weir and V. Bolkhovskiy, "Mutual and self-Inductance in planarized multilayered superconductor integrated circuits: Microstrips, striplines, bends, meanders, ground plane perforations," *IEEE Trans. Appl. Supercond.*, vol. 32, no. 5, pp. 1-31, Aug. 2022, Art. no. 1400331, doi: 10.1109/TASC.2022.3162758.
- [19] J.C. Maxwell, *A Treatise on Electricity & Magnetism*, vol. 2, Chapter XIII section 691, p. 324. Dover Publications Inc., Mineola, NY, USA; unabridged replication of the 3rd ed. Clarendon Press, 1891.
- [20] E.B. Rosa and F.W. Grover, *Formulas and Tables for the Calculation of Mutual and Self-Inductance*, Middletown, Delaware, USA: Leopold Classic Library, 2021.
- [21] F. W. Grover, *Inductance Calculations: working formulas and tables*, Mineola, New York USA: Dover Publications, 2019; originally published: New York: D. Van Nostrand, 1946.
- [22] M.M. Khapaev, "Extraction of inductances of a multi-superconductor transmission line," *Supercond. Sci. Technol.*, vol. 9, pp. 729-733, 1996.
- [23] C. J. Fourie, InductEx, Stellenbosch Univ., Stellenbosch, South Africa, 2015. [Online]. Available: <https://www.sun-magnetics.com/products>
- [24] S.K. Tolpygo, "Scalability of superconductor electronics: Limitations imposed by AC clock and flux bias transformers," submitted to *IEEE Trans. Appl. Supercond.*, *arXiv preprint arXiv:2210.02632*, Oct. 2022, doi: 10.48550/arXiv.2210.02632
- [25] G. Goltsman *et al.*, "Fabrication and properties of an ultrafast NbN hot-electron single-photon detector," *IEEE Trans. Appl. Supercond.*, vol. 11, no. 1, pp. 574-577, March 2001, doi: 10.1109/77.919410.
- [26] A. D. Semenov, G. N. Goltsman and A. A. Korneev, "Quantum detection by current carrying superconducting film," *Physica C*, vol. 351, no. 4, pp. 349-356, Apr. 2001, doi:10.1016/S0921-4534(00)01637-3
- [27] G. N. Goltsman *et al.*, "Picosecond superconducting single-photon optical detector," *Appl. Phys. Lett.*, vol. 79, no. 6, pp. 705-707, Aug. 2001, doi:10.1063/1.1388868
- [28] C. M. Natarajan, M. G. Tanner, and R. H. Hadfield, "Superconducting nanowire single-photon detectors: physics and applications," *Supercond. Sci. Technol.*, vol. 25, no. 6, Art. no. 063001, Apr. 2012, doi:10.1088/0953-2048/25/6/063001
- [29] J. Zmuidzinas, "Superconducting microresonators: Physics and applications," *Annu. Rev. Condens. Matter Phys.*, vol. 3, pp. 169-214, 2012, doi: 10.1146/annurev-conmatphys-020911-125022
- [30] A.C. Anderson, D.J. Lichtenwalner, and W.T. Brogan, *IEEE Trans. Magn.*, vol. MAG 25, p. 2084 (1989).
- [31] D. E. Oates, A. C. Anderson, C. C. Chin, J. S. Derov, G. Dresselhaus and M. S. Dresselhaus, "Surface-impedance measurements of superconducting NbN films," *Phys. Rev. B*, vol. 43, no. 10, pp. 7655-7663, Apr. 1991.
- [32] N. N. Iosad, B. D. Jackson, T. M. Klapwijk, S. N. Polyakov, P. N. Dmitirev, and J. R. Gao, "Optimization of RF- and DC-sputtered NbTiN films for integration with Nb-based SIS junctions," *IEEE Trans. Appl. Supercond.*, vol. 9, no. 2, pp. 1716-1719, June 1999, doi: 10.1109/77.784784.
- [33] Lei Yu *et al.*, "Fabrication of niobium titanium nitride thin films with high superconducting transition temperatures and short penetration lengths," *IEEE Trans. on Appl. Supercond.*, vol. 15, no. 1, pp. 44-48, March 2005, doi: 10.1109/TASC.2005.844126.
- [34] D. J. Thoen, B. G. C. Bos, E. A. F. Haalebos, T. M. Klapwijk, J. J. A. Baselmans, and A. Endo, "Superconducting NbTiN thin films with highly uniform properties over a 100 mm wafer," *IEEE Trans. Appl. Supercond.*, vol. 27, no. 4, pp. 1-5, June 2017, Art. no. 1500505, doi: 10.1109/TASC.2016.2631948.
- [35] S. Miki, M. Takeda, M. Fujiwara1, M. Sasaki1, A. Otomo, and Z. Wang, "Superconducting NbTiN nanowire single photon detectors with low kinetic inductance," *Appl. Phys. Express*, vol. 2, no. 7, 2009, Art. no. 075002.
- [36] M. Schneider, E. Toomley, G. Rowlands, J. Shainline, P. Tschirhart, and K. Segall, "SuperMind: a survey of potential of superconducting electronics for neuromorphic computing," *Supercond. Sci. Technol.*, vol. 35, no.5, Mar. 2022, Art. no. 053001, doi: 10.1088/1361-6668/ac4cd2
- [37] E. Chen, Y. Wang, R. Zhang and N. Yoshikawa, "Design and Implementation of Stochastic Neural Networks Using Superconductor Quantum-Flux-Parametron Devices," *2022 IEEE 35th International*

- System-on-Chip Conference (SOCC)*, 2022, pp. 1-6, doi: 10.1109/SOCC56010.2022.9908075.
- [38] V. K. Semenov, E. B. Golden and S. K. Tolpygo, "A New Family of bioSFQ Logic/Memory Cells," *IEEE Trans. Appl. Supercond.*, vol. 32, no. 4, pp. 1-5, June 2022, Art no. 1400105, doi: 10.1109/TASC.2021.3138369.
- [39] V.K. Semenov, E.B. Golden, and S.K. Tolpygo, "Recent progress with BioSFQ circuit family for neuromorphic computing," *Applied Superconductivity Conference ASC 2022, presentation 2EOr2B-02*